International Journal of Minerals, Metallurgy and Materials
Volume 27, Number 9, September 2020, Page 1295
https://doi.org/10.1007/s12613-020-2009-0

Mechanical properties of graphene nanoplatelets reinforced 7075 aluminum alloy composite fabricated by spark plasma sintering

Hui-min Xia, Lan Zhang, Yong-chao Zhu, Na Li, Yu-qi Sun, Ji-dong Zhang, and Hui-zhong Ma

School of Mechanics and Engineering Science, Zhengzhou University, Zhengzhou 450000, China
(Received: 13 November 2019; revised: 4 February 2020; accepted: 7 February 2020)

Abstract: A 0.3wt% graphene nanoplatelets (GNPs) reinforced 7075 aluminum alloy matrix (7075 Al) composite was fabricated by spark plasma sintering and its strength and wear resistance were investigated. The microstructures of the internal structure, the friction surface, and the wear debris were characterized by scanning electron microscopy, X-ray diffraction, and Raman spectroscopy. Compared with the original 7075 aluminum alloy, the hardness and elastic modulus of the 7075 Al/GNPs composite were found to have increased by 29% and 36%, respectively. The results of tribological experiments indicated that the composite also exhibited a lower wear rate than the original 7075 aluminum alloy.

Keywords: 7075 aluminum alloy; graphene nanoplatelets; spark plasma sintering; strength; wear resistance

1. Introduction

Aluminum alloys comprise a series of materials that are extensively applied in the automotive, aerospace, and electronics fields due to their high strength, high toughness, and low density [1]. As an important and indispensable material in the aviation industry since it was first developed in the 1960s, 7075 aluminum alloy (7075 Al) in particular has reliable properties for the manufacture of aircraft wing spars, aircraft fuselages, and rockets. Despite their wide range of application, aluminum alloys need even higher strength to satisfy the special requirements of industrial applications. In recent years, an increasing number of aluminum-based composites have been introduced to enhance the mechanical properties of the original aluminum-matrix materials. Ramkumar *et al.* [2] investigated the mechanical properties of the 7075 Al/TiC matrix composite prepared using the stir-casting route. The authors found that the bending strength of the 7075 Al/7.5wt% TiC composite was higher than that of the monolithic 7075 Al. Lu *et al.* reported that the 7075 Al hybrid composite, which is reinforced by a mixture of 50vol% SiC_p and 5vol% Cr particles, exhibited lower thermal expansion and higher thermal conductivity than 7075 Al/SiC_p [3].

Graphene, with its single-atomic-layer structure, has outstanding mechanical, thermal, electrical, and magnetic properties. With respect to its mechanical properties, graphene has a Young's modulus of 1.0 TPa, a tensile strength of 130 GPa, and a very low density of 1.06 g/cm^3, and has thus attracted significant interest in its use as a reinforcement material in various composites [4–6]. Elghazaly *et al.* [7] compared the properties of AA2124/3wt% graphene composite with the unreinforced AA2124, the hardness of which was increased by 133%, the wear rate decreased by 34%, and the friction coefficient decreased by 25%. Zhai *et al.* [8] prepared a multilayer graphene-reinforced Ni_3Al matrix composite by the spark plasma sintering method, and found that multilayer graphene can significantly improve the hardness, elastic modulus, and wear resistance of the composite. Meanwhile, both theoretical simulation and experimental performance have proved that graphene provides excellent reinforcement in a metal matrix, polymer matrix, and ceramic matrix composite [9–10]. However, graphene is prone to agglomeration in matrices because of its high specific surface area, which results in unexpected structures and failures to enhance the mechanical properties [11]. Graphene nanoplatelets (GNPs) consist of several graphene layers and the thickness of GNPs ranges from 2.5 to 100 nm. Furthermore, GNPs have properties similar to those of single-layer graphene and uniformly disperse more easily [12–13]. Therefore, GNPs are an excellent candidate for improving the mechanical properties of a composite. For example, the titanium matrix composite with

Corresponding authors: Lan Zhang E-mail: tranquility11@sina.cn; Hui-zhong Ma E-mail: iehzma@zzu.edu.cn

the addition of merely 0.1wt% GNPs has demonstrated a 54.2% higher tensile strength than the original titanium. Based on these studies, the main strengthening factors were reported to be grain refinement, load transfer from the Ti matrix material to the GNPs, and strengthening of the texture of the composite [14]. Shen *et al.* [15] reported that the significant improvement in the tensile strength and flexure properties of a GNPs/epoxy nanocomposite were attained by the addition of GNPs. Berman *et al.* [16] investigated the friction and wear behavior of graphene-lubricated 440C steel and found the coefficient of friction of the graphene-lubricated 440C steel to be reduced to 0.15 compared with that of bare steel (≈1). The wear rate of the steel test pairs also decreased sharply. Nieto *et al.* [17] studied the effects of GNPs on the fracture toughness and wear resistance of alumina ceramics and found them to increase in the composite by 21% and 39%, respectively, compared with unreinforced alumina ceramics. However, as yet few studies have focused on the use of aluminum alloy as the matrix.

Spark plasma sintering (SPS) has many advantages over hot pressing, rolling, spray forming, and other conventional techniques. SPS can synthesize composite materials at a lower temperature and shorter holding time, which contributes to the inhibition of grain growth and realizes grain refinement. Meanwhile, a faster heating rate can reduce the processing time and increase productivity. Therefore, a composite with full density can be sintered in a short time by SPS [18–19].

This paper aims to explore the effect of graphene nanoplatelets (GNPs) on the mechanical properties of the GNPs reinforced 7075 Al alloy matrix (7075 Al/GNPs) composite. We fabricate 7075 Al/GNPs composite using the SPS process and investigate the effect of the addition of GNPs on the relative density, hardness, elastic modulus, and wear resistance of the composite. We discuss the strengthening mechanism based on our observations and analysis of the microstructures.

2. Experimental

2.1. Materials and methods

7075 Al powder with an average particle size of 10 μm and a purity of 99.8% was obtained from Changsha Tianjiu Metal Material Co. Ltd., China. Table 1 lists the chemical compositions of the 7075 Al. GNPs with a purity of 99.5wt%, an average thickness ranging from 4 to 20 nm, and particle sizes ranging from 5 to 10 μm were procured from TIME & NRNO, China.

Table 1. Chemical composition of 7075 Al wt%

Si	Fe	Cu	Mn	Mg	Cr	Zn	Ti	Others	Al
0.4	0.5	1.2–2.0	0.3	2.1–2.9	0.18–0.28	5.1–6.1	0.2	0.15	Bal.

To better disperse GNPs in aluminum alloy powder, GNPs powder was first dispersed in ethanol for 10 min using an ultrasonic process. Aluminum alloy powder was then added to the GNPs solution, which was then exposed to ultrasonic treatment for 30 min. The mixture of 7075 Al and GNPs was then ball milled in a planetary ball mill (XQM-2, Changsha Tianchuang Powder Technology Co. Ltd., China) for 2 h at 200 r/min at a ball-to-powder mass ratio of 4:1. The powders were mixed to a pulp by mechanical stirring in water baths for 3 h at 60°C and were subsequently dried at 80°C for 3 h in a tubular oven (GSL 1400X, Hefei Kejing Material Technology Co. Ltd., China) in an argon atmosphere.

2.2. Preparation of 7075 Al/GNPs

Powder mixtures containing 0.3wt% GNPs were sintered using an SPS process (SPS-10T-5, Shanghai Chenhua Electric Furnace Co. Ltd., China) with a graphite mold. The samples were sintered at 550°C at a heating rate of 50°C/min and a pressure of 50 MPa for a holding time of 6 min, and were then cooled in the furnace by a water circulation system. The temperature was measured via a thermocouple inserted into a hole on the outside surface of the graphite mold. The current was direct current (DC) pulsed using a 5 ms on/5 ms off pulse profile. The size of the sintered compact cylinder was ϕ20 mm × 5 mm. Three specimens were prepared using the process described above.

2.3. Characterization

The densities of the sintered compacts were measured using Archimedes' method with distilled water. We first measured the density of the distilled water at the experimental ambient temperature. After polishing with grinding papers of different grits (500, 800, 1000-grit, in that order), we determined the hardness of the sintered compact using a Vickers hardness tester (HXD-1000TMC, Shanghai Taiming Optical Instrument Co. Ltd., China) under a load of 1.96 N for a dwell time of 15 s. We averaged the values obtained by five measurements of each material. Elastic modulus tests were conducted using an NHT2 Nano-indentation test system with Berkovich indenters.

Wear resistance tests were conducted using a tribometer (Model MS-T3000; Lanzhou Institute of Chemical Physics, Chinese Academy of Sciences, China) under a load of 0.98 N at 200 r/min for 30 min against a 4-mm-diameter stainless steel grinding ball (GCr15) as the counter surface.

We observed the microstructure of the composite and the surface morphology of the wear debris by scanning electron microscopy (SEM, Zeiss, Auriga FIB, Germany) with an ac-

celerating voltage of 15 kV. Phase compositions were identified by X-ray diffraction (XRD, Panalytical, Empyrean, Netherlands) at 40 mA and 45 kV and a step size of 0.02° using Cu K_α radiation.

3. Results and discussion

3.1. XRD analysis

Fig. 1 shows the XRD patterns of the 7075 Al/GNPs composite and the original 7075 Al, in which no characteristic peak of Al_4C_3 or other metallic carbides are detected. On one hand, the SPS process has an efficient self-cleaning ability that reduces the formation of the second phase. On the other hand, the surfaces of particles may be covered with a thin oxide film, which inhibits the formation of metallic carbides. We calculated the grain sizes of the original 7075 Al and the composite using the Scherrer formula. The results indicate that the grain size of the composite had decreased significantly to 76 nm compared with the grain size of the original 7075 Al, 106 nm, which confirmed that the addition of GNPs served to refine the grain size and optimize the internal microstructure.

3.2. SEM analysis

The micrograph in Fig. 2(a) shows that the raw aluminum alloy particles have a spherical morphology with diameters of roughly 10 μm. The raw GNPs particles were found to have a sheet-like morphology that tends to occur in stacked multilayers, as shown in Fig. 2(b). Fig. 2(c) shows an image

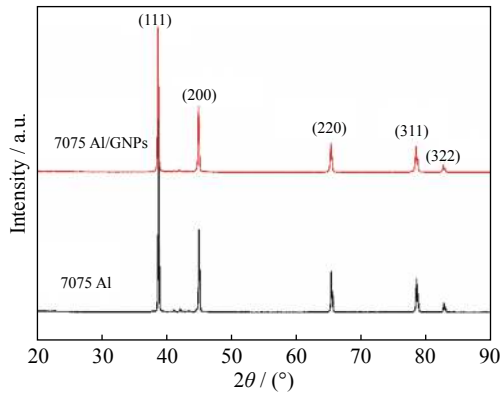

Fig. 1. XRD spectra of the 7075 Al and the 7075 Al/GNPs composite after sintering.

of the mixture of GNPs and aluminum alloy powders obtained by ultrasonic dispersion, ball grinding, and drying, in which a few clusters of GNPs are distributed in the aluminum alloy powder. This proves that the aluminum alloy powder undergoes a change from regular to irregularly shaped spheres. It is clear from Fig. 2(d) that the GNPs (outlined by red circles) are homogeneously dispersed in the aluminum alloy matrix.

3.3. Raman analysis

Fig. 3 shows the Raman spectra of pure GNPs and the 7075 Al/GNPs composite, which differ significantly. The results reveal that there is a D-band at around 1350 cm^{-1} in the spectrum of the composite, and the D peak is linked to de-

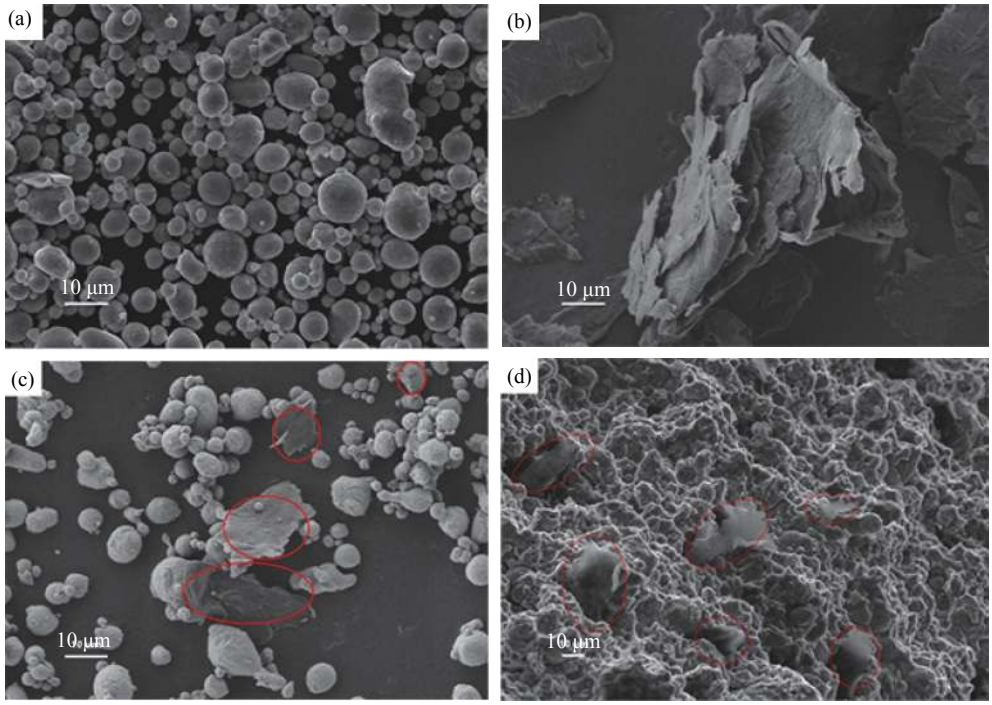

Fig. 2. SEM images of (a) raw 7075 Al powder, (b) raw GNPs powder, (c) mixed powder, and (d) fracture surface of the 7075 Al/GNPs composite.

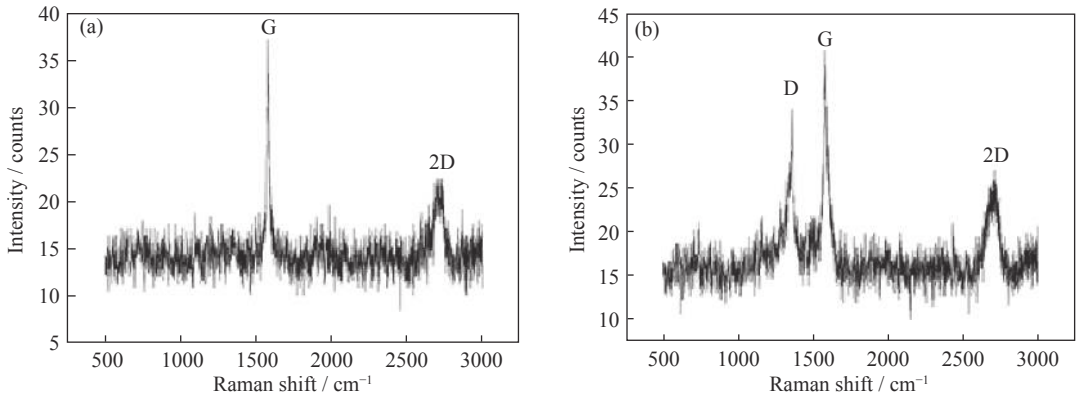

Fig. 3. Raman spectra of (a) the raw GNPs powder and (b) the 7075 Al/GNPs composite.

fects in the graphene structure. The emergence of a D band illustrates that the use of high-energy ball milling and SPS to produce composite specimens destroys the graphene's perfect structure to some extent.

3.4. Mechanical properties

We determined the mass of the specimens in air and water separately and used the Archimedes method to determine their densities. Table 2 lists the densities of the two specimens. The addition of the GNPs may slightly reduce the actual and relative densities due to the fact that GNPs easily absorb gas elements such as oxygen and nitrogen, which increases the porosity of the composite to a certain extent and reduces the relative density.

Table 2. Densities of the 7075 Al and the 7075 Al/GNPs composite

Specimen	Actual density / (g·cm^{-3})	Theoretical density / (g·cm^{-3})	Relative density
7075 Al	2.6781	2.8100	0.9531
7075 Al/GNPs	2.6714	2.8034	0.9529

Fig. 4 shows the Vickers hardness and elasticity modulus values of the 7075 Al and the 7075 Al/GNPs composite. Both the Vickers hardness and elasticity modulus of the composite were found to be higher than those of the 7075 Al. The values for the composite were HV 124.9 and 135 GPa, respectively, which are 29% and 36% higher than those of the 7075 Al. The results clearly indicate that GNPs provide a highly effective reinforcement of the 7075 Al matrix. The dispersal of GNPs in the matrix also serves to refine the grain sizes by grain boundary pinning, which increases the hardness of the composite. The XRD analysis above also indicates that the addition of GNPs refines the grain size, which improves the strength of the composite [20]. The matrix and GNPs have a significant mismatch in their coefficients of thermal expansion, which leads to an increase in the dislocation density of the matrix. The presence of GNPs also inhibits dislocation in the aluminum alloy matrix. Both these factors result in the increased strength of the composite. The wrinkled morphology of GNPs is also favorable for mechanical bonding between the matrix and GNPs. A good interfacial bonding is known to efficiently facilitate load transfer and improve the composite strength [21–22].

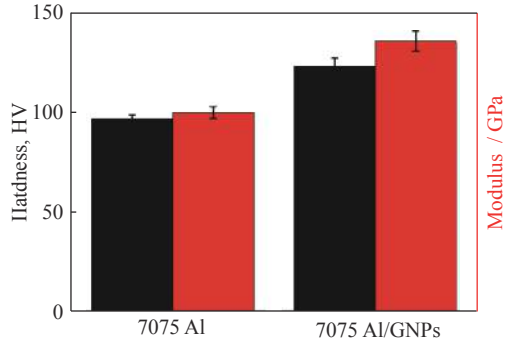

Fig. 4. Vickers hardness and elasticity modulus values of the 7075 Al and the 7075 Al/GNPs composite.

Fig. 5 shows the variation in the friction coefficient of the 7075 Al and the 7075 Al/GNPs composite over the same period of time. It is evident that the friction coefficient of the 7075 Al/GNPs composite is much lower than that of the 7075

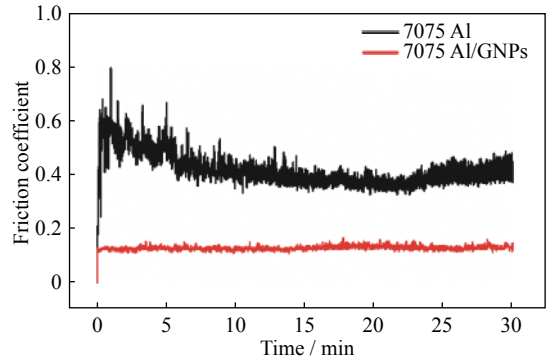

Fig. 5. Friction coefficients of the 7075 Al and 7075 Al/GNPs composite.

Al. In addition, under the same wear test conditions, the wear rate of the 7075 Al/GNPs composite is 0.00273 $mm^3/(N \cdot m)$, while that of 7075 Al is 0.00342 $mm^3/(N \cdot m)$. The 7075 Al/GNPs composite shows better wear resistance. Thus, the addition of GNPs is advantageous to the wear resistance of the composite.

To investigate the tribological mechanism of the composite, the surface morphologies of the wear scars of the 7075 Al and the 7075 Al/GNPs composite are shown in Fig. 6. The surface of the wear scar of the 7075 Al exhibits delamination and massive exfoliation, which can cause severe wear. The worn surface of the 7075 Al/GNPs composite is smoother than that of the 7075 Al, which contributes to a lower wear rate of the composite. In addition, the Archard equation demonstrates that the wear rate is inversely proportional to the hardness of the sample, although it does not account for any effect from the microstructure of a material [23–24]. This can explain why the composite exhibits a lower wear rate than the 7075 Al.

On the worn surface of the 7075 Al (Fig. 6(a)), big flake debris had formed and its removal from the friction surface lessens the actual contact area between the friction surface and grind ball, which tends to increase the friction coefficient [25]. In contrast, the composite has a smaller grain size because of the addition of GNPs (as confirmed by the XRD results), which can effectively resist deformation of the friction surface, thus reducing the friction coefficient and wear rate [24]. Besides, it is speculated that the graphene film that forms on the worn surface of the composite decreases the direct contact between the matrix and grinding ball, which results in a decrease in the friction coefficient of the 7075 Al/GNPs composite [26].

Fig. 7 shows the topographies of the wear debris of the 7075 Al and the 7075 Al/GNPs composite. The SEM images of the abrasive particles reveal that the wear debris of both the 7075 Al and the 7075 Al/GNPs composite have a flake-like structure. The average particle size of the wear debris of the 7075 Al/GNPs composite is smaller than that of the 7075 Al, which is conducive to the lower wear rate of the composite.

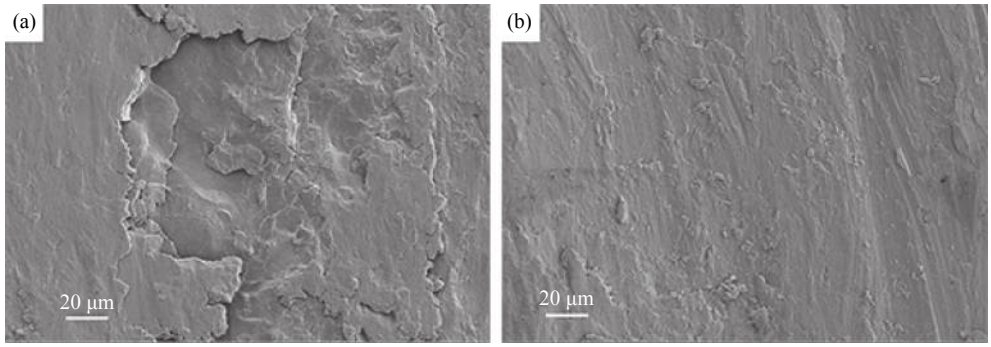

Fig. 6. Friction surface of (a) the 7075 Al and (b) the 7075 Al/GNPs composite.

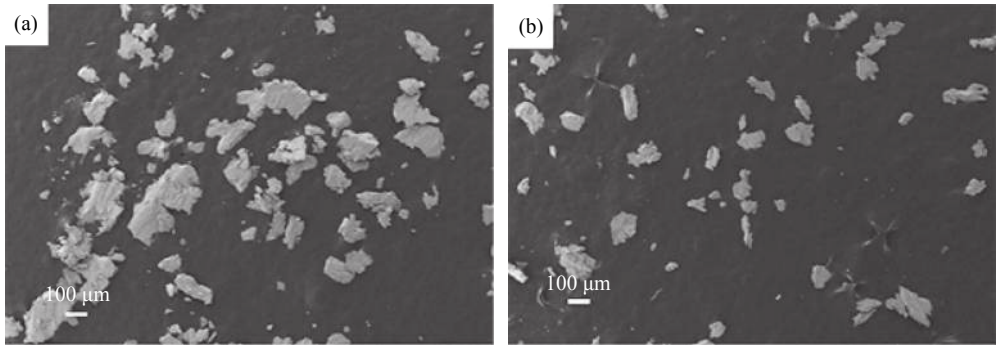

Fig. 7. SEM images of wear debris of (a) the 7075 Al and (b) the 7075 Al/GNPs composite.

Based on the above results, the apparent improvement in the wear resistance of the 7075 Al/GNPs composite can be attributed to the following factors: the addition of GNPs is favorable for refining the grain size and improving the mechanical properties; GNPs have excellent lubricity and thus enhance the abrasion resistance; the hardness of the 7075 Al/GNPs composite was found to be higher than that of the 7075 Al; severe plastic deformation occurs in unreinforced 7075 Al, which leads to a higher wear rate.

4. Conclusions

(1) A GNPs-reinforced 7075 Al composite was successfully produced using a SPS process.

(2) The addition of graphene was found to significantly refine the grain size and the mechanical properties of the alu-

minum alloy. Compared with the original 7075 Al, the hardness and elasticity modulus of the composite increased by 29% and 36%, respectively.

(3) The density of the 7075 Al/GNPs composite was found to be lower than that of the 7075 Al, which is conducive to increasing the specific strength of the composite.

(4) In terms of wear resistance, the 7075 Al/GNPs composite was found to have a lower wear rate than the 7075 Al.

Acknowledgement

This work was financially supported by the Program for New Century Excellent Talents in University (No. NCET-11-0951).

References

[1] J. Suthar and K.M. Patel, Processing issues, machining, and applications of aluminum metal matrix composites, *Mater. Manuf. Process.*, 33(2018), No. 5, p. 499.

[2] K.R. Ramkumar, S. Sivasankaran, F.A. Al-mufadi, S. Siddharth, and R. Raghu, Investigations on microstructure, mechanical, and tribological behaviour of AA7075–*x* wt.% TiC composites for aerospace applications, *Arch. Civ. Mech. Eng.*, 19(2019), No. 2, p. 428.

[3] T.W. Lu, W.P. Chen, P. Wang, M.D. Mao, Y.X. Liu, and Z.Q. Fu, Enhanced mechanical properties and thermo-physical properties of 7075Al hybrid composites reinforced by the mixture of Cr particles and SiC_p, *J. Alloys. Compd.*, 735(2018), p. 1137.

[4] A.K. Kasar, G.P. Xiong, and P.L. Menezes, Graphene-reinforced metal and polymer matrix composites, *JOM*, 70(2018), No. 6, p. 829.

[5] S. Baskut, A. Cinar, and S. Turan, Directional properties and microstructures of spark plasma sintered aluminum nitride containing graphene platelets, *J. Eur. Ceram. Soc.*, 37(2017), No. 12, p. 3759.

[6] F.Y. Chen, J.M. Ying, Y.F. Wang, S.Y. Du, Z.P. Liu, and Q. Huang, Effects of graphene content on the microstructure and properties of copper matrix composites, *Carbon*, 96(2016), p. 836.

[7] A. Elghazaly, G. Anis, and H.G. Salem, Effect of graphene addition on the mechanical and tribological behavior of nanostructured AA2124 self-lubricating metal matrix composite, *Composites Part A*, 95(2017), p. 325.

[8] W.Z. Zhai, X.L. Shi, J. Yao, A.M.M. Ibrahim, Z.S. Xu, Q.S. Zhu, Y.C. Xiao, L. Chen, and Q.X. Zhang, Investigation of mechanical and tribological behaviors of multilayer graphene reinforced Ni_3Al matrix composites, *Composites Part B*, 70(2015), p. 149.

[9] D.B. Xiong, M. Cao, Q. Guo, Z.Q. Tan, G.L. Fan, Z.Q. Li, and D. Zhang, High content reduced graphene oxide reinforced copper with a bioinspired nano-laminated structure and large recoverable deformation ability, *Sci. Rep.*, 6(2016), art. No. 33801.

[10] S.W. Chang, A.K. Nair, and M.J. Buehler, Nanoindentation study of size effects in nickel-graphene nanocomposites, *Philos. Mag. Lett.*, 93(2013), No. 4, p. 196.

[11] W.M. Tian, S.M. Li, B. Wang, X. Chen, J.H. Liu, and M. Yu, Graphene-reinforced aluminum matrix composites prepared by spark plasma sintering, *Int. J. Miner. Metall. Mater.*, 23(2016), No. 6, p. 723.

[12] M. Prasad, T.N. Rao, P.S.R. Prasad, and D.S. Babu, Preparation of bulk graphene nanoplatelets by spark plasma sintering — electrical and thermal properties, *Int. J. Nanosci.*, 15(2016), No. 05n06, art. No. 1660003.

[13] T. Borkar, H. Mohseni, J. Hwang, T. Scharf, J. Tiley, S.H. Hong, and R. Banerjee, Spark plasma sintering (SPS) of carbon nanotube (CNT)/graphene nanoplatelet (GNP)-nickel nanocomposites: Structure property analysis, [in] T. Sano and T. S. Srivatsan eds., *Advanced Composites for Aerospace, Marine, and Land Applications II*, The Minerais, Metals & Materials Society, Springer, Cham, 2015, p. 53.

[14] X.N. Mu, H.M. Zhang, H.N. Cai, Q.B. Fan, Z.H. Zhang, Y. Wu, Z.J. Fu, and D.H. Yu, Microstructure evolution and superior tensile properties of low content graphene nanoplatelets reinforced pure Ti matrix composites, *Mater. Sci. Eng. A*, 687(2017), p. 164.

[15] M.Y. Shen, T.Y. Chang, T.H. Hsieh, Y.L. Li, C.L. Chiang, H. Yang, and M.C. Yip, Mechanical properties and tensile fatigue of graphene nanoplatelets reinforced polymer nanocomposites, *J. Nanomater.*, 2013(2013), art. No. 565401.

[16] D. Berman, A. Erdemir, and A.V. Sumant, Reduced wear and friction enabled by graphene layers on sliding steel surfaces in dry nitrogen, *Carbon*, 59(2013), p. 167.

[17] A. Nieto, J.M. Zhao, Y.H. Han, K.H. Hwang, and J.M. Schoenung, Microscale tribological behavior and in vitro biocompatibility of graphene nanoplatelet reinforced alumina, *J. Mech. Behav. Biomed. Mater.*, 61(2016), p. 122.

[18] Z.A. Munir, U. Anselmi-Tamburini, and M. Ohyanagi, The effect of electric field and pressure on the synthesis and consolidation of materials: A review of the spark plasma sintering method, *J. Mater. Sci.*, 41(2006), No. 3, p. 763.

[19] T.T. Liu, X.B. He, Q. Liu, S.B. Ren, L. Zhang, and X.H. Qu, Preparation and thermal conductivity of spark plasma sintered aluminum matrix composites reinforced with titanium-coated graphite fibers, *Adv. Eng. Mater.*, 17(2015), No. 4, p. 502.

[20] A. Nieto, D. Lahiri, and A. Agarwal, Graphene nanoplatelets reinforced tantalum carbide consolidated by spark plasma sintering, *Mater. Sci. Eng. A*, 582(2013), p. 338.

[21] M. Rashad, F. Pan, A. Tang, and M. Asif, Effect of graphene nanoplatelets addition on mechanical properties of pure aluminum using a semi-powder method, *Prog. Nat. Sci. Mater. Int.*, 24(2014), No. 2, p. 101.

[22] G. Li and B.W. Xiong, Effects of graphene content on microstructures and tensile property of graphene-nanosheets / aluminum composites, *J. Alloys Compd.*, 697(2017), p. 31.

[23] A. Bahrami, N. Soltani, and M.I. Pech-canul, Effect of sintering temperature on tribological behavior of Ce-TZP/Al_2O_3 -aluminum nanocomposite, *J. Compos. Meter.*, 49(2015), No. 28, p. 3507.

[24] R. Deaquino-lara, N. Soltani, A. Bahrami, E. Gutiérrez-castañeda, E. García-sánchez, and M.A.L. Rodríguez, Tribological characterization of Al7075–graphite composites fabricated by mechanical alloying and hot extrusion, *Mater. Des.*, 67(2015), p. 224.

[25] N. Soltani, H.R. Jafari Nodooshan, A. Bahrami, M.I. Pech-canul, W.C. Liu, and G.H. Wu, Effect of hot extrusion on wear properties of Al–15 wt.% Mg_2Si *in situ* metal matrix composites, *Mater. Des.*, 53(2014), p. 774.

[26] M. Tabandeh-khorshid, E. Omrani, P.L. Menezes, and P.K. Rohatgi, Tribological performance of self-lubricating aluminum matrix nanocomposites: Role of graphene nanoplatelets, *Eng. Sci. Technol. Int. J.*, 19(2016), No. 1, p. 463.